Title	Characteristics of Brittle Fracture under General Combined Modes(Welding Mechanics, Strength & Design)
Author(s)	Ueda, Yukio; Ikeda, Kazuo; Yao, Tetsuya; Aoki, Mitsuru; Shibasaki, Shunichi
Citation	Transactions of JWRI. 9(2) P.237-P.246
Issue Date	1980-12
Text Version	publisher
URL	http://hdl.handle.net/11094/12104
DOI	
rights	本文データはCiNiiから複製したものである
Note	

Characteristics of Brittle Fracture under General Combined Modes†

Yukio UEDA*, Kazuo IKEDA**, Tetsuya YAO***, Mitsuru AOKI**** and Shun-ichi SHIBASAKI *****

Abstract

In the previous papers, the brittle fracture initiation characteristics of plates with an inclined crack under bi-axial tension were studied. This condition led to the brittle fracture under the combination of opening (Mode I) and sliding (Mode II) modes. In this paper, brittle fracture under all possible combination of opening, sliding and tearing (Mode III) modes is investigated both theoretically and experimentally.

Using specimens of PMMA (Polymethylmethacrylate), fracture tests under pure Mode II, pure Mode III, the combination of Modes I and III, and that of Modes I, II and III are carried out. Then the test results are compared with those predicted by the fracture criteria which are represented in terms of : (1) maximum tangential stress, $[\sigma_\theta]_{max}$, (2) maximum energy release rate at the propagation of a small kinked crack, $[G^k(\gamma)]_{max}$, and (3) maximum energy release rate at the initiation of a small kinked crack, $[G(\gamma)]_{max}$.

The following conclusions are drawn from the results of the investigation.

(1) The measured fracture stresses under an arbitrary combination of the crack surface displacement modes are in good agreement with those predicted by $[G^k(\gamma)]_{max}$ or $[G(\gamma)]_{max}$ criterion. These energy release rates are expressed in the closed forms, and can be applied to any crack under any combination of the lodes.

(2) Although $[\sigma_\theta]_{max}$ criterion may be used for fracture under any combined modes including Mode III, this is not effective except for the combinations of Modes I and II.

(3) The interaction curves of brittle fracture strength under any arbitrary combenations of Modes I, II, and III are obtained based on $[G^k(\gamma)]_{max}$ and $[G(\gamma)]_{max}$ criteria.

KEY WORDS: (Brittle Fracture) (Mild Steel) (Unfired Pressure Vessels) (Toughness) (Propagation of Cracks)

1. Introduction

Cracks in actual structures are generally under the combined stress modes, and it is very important to clarify the characteristics of brittle fracture initiation under the combined stress modes for design of fracture safe structures. The authors have been investigated, under combination of Mode I (Opening Mode) and II (Sliding Mode), the initiation characteristics of perfectly brittle fracture[1)2)], brittle fracture with small scale yeilding[1)2)] and that with large scale yeilding or general yielding[3)4)].

In this paper, the initiation characteristics of prefectly brittle fracutre under pure Mode II, pure Mode III, the combination of Modes I and III, and that of Modes I, II and III are investigated. First, several existing criteria for brittle fracture initiation under the combination of Modes I, II and III are examined, and the strain energy release rate at the initiation of a small kinked crack under such combined stress modes is derived. Then, a series of fracture tests under various combined modes is carried out using PMMA specimens. The test results are compared with those predicted by the fracture criteria which are represented in terms of : (1) maximum tangential stress, $[\sigma_\theta]_{max}$, (2) maximum strain energy release rate at the propagation of a small kinked crack, $[G^k(\gamma)]_{max}$, and (3) maximum strain energy release rate at the propagation of a small kinked crack, $[G(\gamma)]_{max}$. Furthermore, the interaction curves of the brittle fracture strength under arbitrary combination of Modes I, II and III are obtained based on $[G^k(\gamma)]_{max}$ and $[G(\gamma)]_{max}$ criteria.

† Received on September 24, 1980

* Professor
** General Manager, Mechanical Engineering Research Laboratory, Kobe Steel Ltd.
*** Associate Professor, Faculty of Engineering, Hiroshima University
**** Research Engineer, Structural Engineering Laboratory, Kobe Steel Ltd.
***** Graduate Student (Presently, Toyota Automobile Ltd.)

Transactions of JWRI is published by Welding Research Institute of Osaka University, Suita, Osaka, Japan

2. Brittle Fracture Criteria under Combined Modes I, II and III

2.1 Criterion based on the maximum tangential stress, $[\sigma_\theta]_{max}$

First, the maximum tangential stress criterion under the combined modes of I and II is considered. Employing the coordinate system shown in **Fig. 1 (a)**, the tangential stress, σ_θ, near the tip of the crack is expressed as follows.

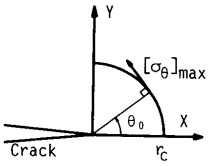

(a) Combined modes of I and II

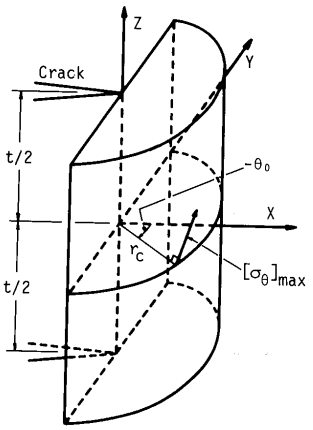

(b) Combined modes of I, II and III

Fig. 1 Maximum tangential stress

$$\sigma_\theta = \frac{1}{2\sqrt{2\pi r}} \cos\frac{\theta}{2}\left\{K_I(1+\cos\theta) - 3K_{II}\sin\theta\right\}$$

$$+\sigma_x \sin^2\theta + \sqrt{2r/c}\, f(K_I, K_{II}, \theta) \qquad (1)$$

where

K_I, K_{II} ; Stress intensity factors for Mode I and II, respectively

σ_x ; Uniform stress in x-direction

The third term in Eq. (1) is a negligibly small quantity.

The maximum tangential stress criterion indicates that the fracture initiates in the direction of the maximum tangential stress, $[\sigma_\theta]_{max}$, when $[\sigma_\theta]_{max}\sqrt{r}$ reaches to the critical value[5)6)]. In this direction, the shear stress, $\tau_{r\theta}$, is zero. The second term in Eq. (1) plays an important role when the direction of the initial crack propagation is considered, and the results changes depending on the distance, r_c, where the stress, σ_θ, is considered[1)2)6)].

If the second and the third term in Eq. (1) are neglected, this criterion coincides with the stress intensity factor criterion. The components of the stress intensity factor, $K_{I\theta}$ and $K_{II\theta}$, in the direction, θ, from the crack tip can be expressed in the following form.

$$K_{I\theta} = \frac{1}{2}\cos\frac{\theta}{2}\left\{K_I(1+\cos\theta) - 3K_{II}\sin\theta\right\}$$

$$K_{II\theta} = \frac{1}{2}\cos\frac{\theta}{2}\left\{K_I\sin\theta + K_{II}(3\cos\theta - 1)\right\} \qquad (2)$$

This criterion indicates that the fracture initiates in the direction of $K_{II\theta} = 0$, when $K_{I\theta}$ reaches to the critical value.

The above mentioned fracture criterion under the combination of Modes I and II can be extended to that under the combination of modes I, II and III. Strictly speaking, a three dimensional stress analysis is required in this case. However, as such analysis is very complicated, an approximate analysis is performed assuming that the deformations and stresses are uniform in the direction of the plate thickness.

Under the combination of Modes I and II, the direction of the maximum tangential stress, $[\sigma_\theta]_{max}$, coincides with that of no shear stress. This indicates that $[\sigma_\theta]_{max}$ is the principal stress, and the line normal to $[\sigma_\theta]_{max}$ passes through the origin of the coordinate. Therefore, it may also be said that the crack initiates in the direction which the line normal to the principal stress on the circle of radius r_c passes through the origin of the coordinate as shown in Fig. 1 (a). To extend this concept to the combination of Modes I, II and III, the coordinate system shown in **Fig. 1 (b)** is employed. Among the principal stresses on the circle of radius r_c shown in Fig. 1 (b), the one which the line normal to the principal stress passes through the origin of the coordinate is the maximum tangential stress, $[\sigma_\theta]_{max}$, under the combination of Modes I, II and III. The crack propagation initiates when $[\sigma_\theta]_{max}$ reaches to the critical value. In this case, the angle, θ_0, in Fig. 1 (b) seems to have no physical meaning, and only the magnitude of $[\sigma_\theta]_{max}$ is important.

2.2 Criterion based on the minimum strain energy density factor, S_{min}

The strain energy, ΔW, stored in the small element, ΔA, in the vicinity of the tip of the crack can be expressed as follows.

$$\Delta W/\Delta A = [\, S/r + (\text{non-singular terms})\,] \qquad (3)$$

$$S = a_{11}K_I^2 + 2a_{12}K_IK_{II} + a_{22}K_{II}^2 + a_{33}K_{III} \qquad (4)$$

where a_{ij} is the function of material constants and θ. S represented by Eq. (4) is the strain energy density factor. Minimum strain energy density factor criterion indicates that the crack propagation initiates in the direction of the minimum strain energy density factor, S_{min}, when S_{min} reaches to the critical value. This criterion was proposed by G. Sih[7], but the physical meaning of this criterion is doubtfull.

2.3 Criterion based on the maximum strain energy release rate at the propagation of a small kinked crack, $[G^k(\gamma)]_{max}$

Several papers are reported as to the stress intensity factors at the tip of the kinked crack as shown in **Fig. 2**. Bilby and Cardew[8] derived the stress intensity factors of a kinked crack, $K_I(\gamma)$ and $K_{II}(\gamma)$, numerically, based on the expression derived by Khrapkov[9]. Chatterjee[10] and Hussain[11] also derived such stress intensity factors under combined modes of I and II employing the complex stress function. Here, the results by Hussain[11] are shown, which are in the closed form as follows.

$$K_I(\gamma) = \left(\frac{4}{3+\cos^2\gamma}\right)\left(\frac{1-\gamma/\pi}{1+\gamma/\pi}\right)^{\gamma/2\pi}\left(K_I\cos\gamma + \frac{3}{2}K_{II}\sin\gamma\right) \tag{5}$$

$$K_{II}(\gamma) = \left(\frac{4}{3+\cos^2\gamma}\right)\left(\frac{1-\gamma/\pi}{1+\gamma/\pi}\right)^{\gamma/2\pi}\left(K_{II}\cos\gamma - \frac{1}{2}K_I\sin\gamma\right)$$

Sih[12] and Smith[13] also derived the stress intensity factor of Mode III for a kinked crack, which is expressed in the following form.

$$K_{III}(\gamma) = \left(\frac{1-\gamma/\pi}{1+\gamma/\pi}\right)^{\gamma/2\pi} K_{III} \tag{6}$$

When the kinked crack propagates in the kinked direction, the strain energy release rate, $G^k(\gamma)$, can be expressed as follows.

$$G^k(\gamma) = \frac{1-\nu^2}{E}\left\{K_I(\gamma)^2 + K_{II}(\gamma)^2 + \frac{1}{1-\nu}K_{III}(\gamma)^2\right\} \tag{7}$$

This criterion indicates that crack propagation initiates in the direction of the maximum strain energy release rate, $[G^k(\gamma)]_{max}$, when $[G^k(\gamma)]_{max}$ reaches to the critical value.

2.4 Criterion based on the maxmum strain energy release rate at the initiation of a small kinked crack, $[G(\gamma)]_{max}$

In the previous papers[1)2)], a special attention was paid to a crack which propagates in the direction, γ, from the tip of the crack, and the strain energy release rate, $G(\gamma)$, was calculated for the crack under the combination of Modes I and II using the finite element method. However, in the case of the combined modes of I, II and III, the calculation requires the three dimensional stress analysis, which is very complicated and time consuming. In this report, an approximate analytical method is employed for calculation of $G(\gamma)$. That is, $G(\gamma)$ is calculated as the work to close the gap produced along the infinitesimal small kinked part of the kinked crack. This work can be evaluated with the stresses which are induced near the tip of the main crack when only the main crack exists and the crack opening displacements of the kinked part of the crack shown in **Fig. 2.** Assuming that the crack opening

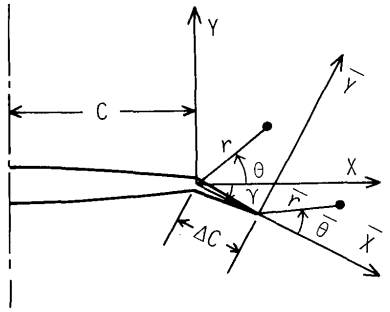

Fig. 2 Configuration of kinked crack

displacements of the infinitesimally small kinked crack can be represented by $K_I(\gamma)$, $K_{II}(\gamma)$ and $K_{III}(\gamma)$ as in the case of an usual single crack, the strain energy release rate, $G(\gamma)$, can be expressed in the following from,

$$G(\gamma) = \frac{1-\nu}{4G}\left(\frac{4}{3+\cos^2\gamma}\right)\left(\frac{1-\gamma/\pi}{1+\gamma/\pi}\right)^{\gamma/2\pi}\cos\frac{\gamma}{2}K_I^2 \times \left(\cos\gamma + \frac{1}{2} + \frac{1}{2}\cos^2\gamma\right) + 2K_IK_{II}\sin\gamma\left(1+\cos\gamma\right) + K_{II}^2\left(-\frac{3}{2}\cos^2\gamma - \cos\gamma + \frac{9}{2}\right) + \frac{1}{2G}\left(\frac{1+\gamma/\pi}{1+\gamma/\pi}\right)^{\gamma/2\pi}\cos\frac{\gamma}{2}K_{III}^2 \tag{8}$$

where G and ν are the shear modulus and Poisson's ratio, respectively, when $\gamma = 0$, Eq. (8) reduces to the well known form of the strain energy release rate as follows.

$$[G(\gamma)]_{\gamma=0} = \frac{1-\nu}{2G}\left[K_I^2 + K_{II}^2 + \frac{1}{1-\nu}K_{III}^2\right] \tag{9}$$

The strain energy release rate expressed by Eq. (9) is the one when the crack propagates in the direction of the initial crack line.

3. Fracture Test

3.1 Material of the specimen

The test specimens are made of PMMA, which shows a perfectly brittle behavior at room temperature. The thickness of the PMMA plate is 10 mm, and its mechanical properties are shown in **Table 1**.

Table 1 Mechanical properties of PMMA

E (kg/mm^2)	ν	σ_B (kg/mm^2)
320	0.35	8.0

3.2 Test specimens

The configuration of the test specimens for various combined mode tests are shown in **Figs. 3, 4, 5** and **6**. The stress intensity factors, K_I, K_{II} and K_{III}, for the notch in each test specimen are summarized in **Table 2**.

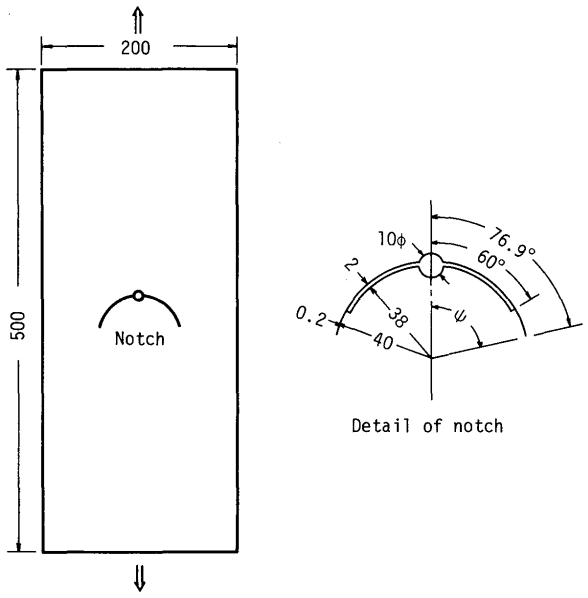

Fig. 3 Plate specimen with a curvilinear crack (for pure mode II test)

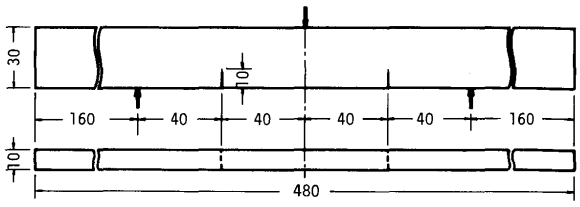

(a) Test specimen for Mode II test

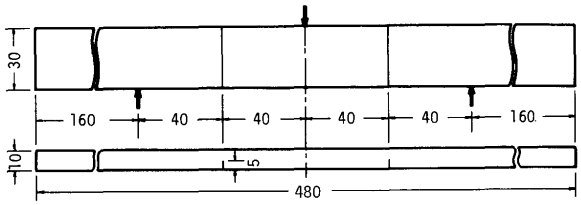

(b) Test specimen for Mode III test

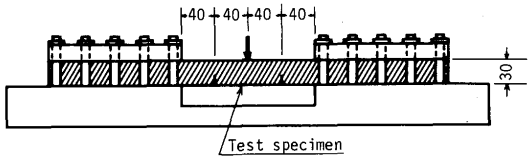

(c) Loading apparatus

Fig. 4 Beam specimen for pure shear test

Figure 3 shows the plate specimen with a curvilinear notch for pure Mode II test. The angle of the curvilinear crack, ψ, is so chosen as the stress intensity factor of Mode I, K_I, vanishes. The stress intensity factors of the curvilinear cracks are derived by Sih[14], but his results contain an error. Hussain[15] corrected the results, which are shown in Table 2. According to his results, K_I becomes zero when $\psi = 76.9°$. (This angle is misprinted as 79.6° in Ref. 11))

Figure 4 (a) and (b) show beam type specimens for pure Mode II and Mode III tests, respectively. Bending load is so applied as shown in Fig. 4 (c) with the condition of both ends fixed, and the notches are machined at the section where the bending stress becomes zero. Though the distribution of the shear stress at the section of the beam specimen is in a parabola type, the mean shear stress, τ, is employed when the stress intensity factors, K_{II} and K_{III} are calculated.

Figure 5 (a) and (b) show the straight side specimen and the cruciform specimen, respectively, for test under the combined modes of I and III. Figure 6 also shows the straight side specimen for tests under the combined modes of I, II and III, of which notch is inclined at angles α and β to the loading direction as illustrated in the figure.

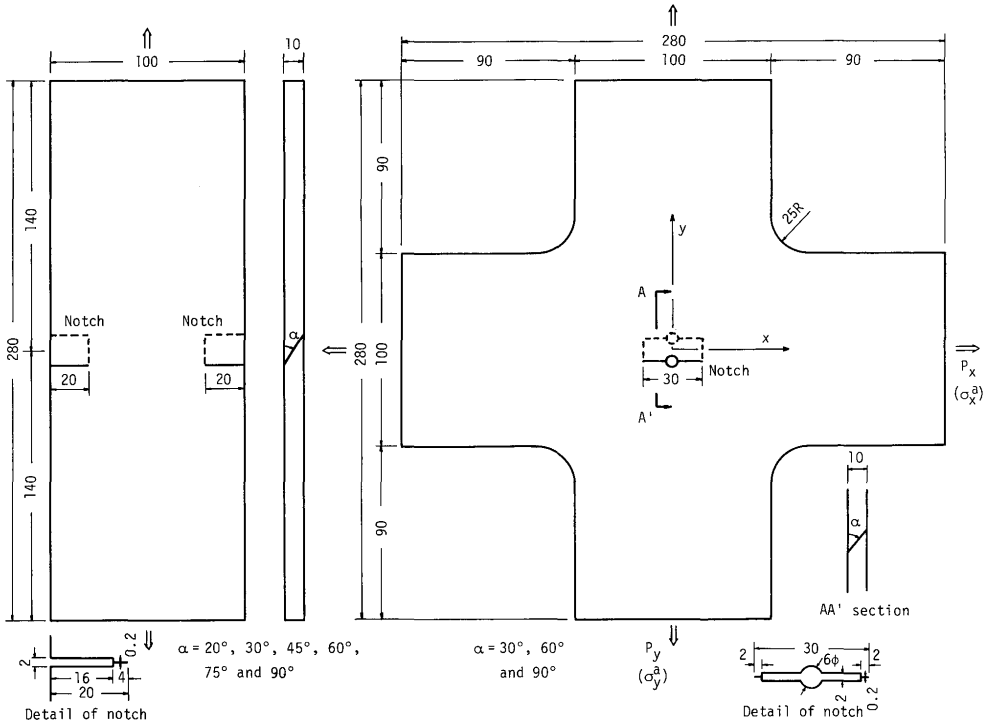

Fig. 5 Plate specimen for test under combined modes of I and III

Table 2 Formulas used to calculate K-value of test specimens

Mode	Test specimen	K - value
I	Fig.5 (a) ($\alpha = 90°$)	$K_I = \sigma\sqrt{\pi c}\sqrt{\frac{2b}{\pi c}}\left(\tan\frac{\pi c}{2b} + 0.1\sin\frac{\pi c}{b}\right)$ (10) where σ : applied stress c : length of edge notch b : half width of specimen
II	Fig.3	$K_I = \frac{1}{2}\sigma\sqrt{\pi R\sin\psi}\cos\frac{\psi}{2}\frac{-3\cos^4(\psi/2) + 10\cos^2(\psi/2) - 5}{2 - \cos^2(\psi/2)}$ $K_{II} = -\frac{1}{2}\sigma\sqrt{\pi R\sin\psi}\sin\frac{\psi}{2}\frac{-3\cos^4(\psi/2) + 8\cos^2(\psi/2) - 1}{2 - \cos^2(\psi/2)}$ (11) where R : radius of circular arc ψ : half central angle of sector
	Fig.4 (a)	$K_{II} = \tau\sqrt{\pi c}$ (12) where τ : mean shear stress at beam section
III	Fig.4 (b)	$K_{III} = \tau\sqrt{\pi c}$ (13)
I + III	Fig.5	$K_I = \sigma_y^\infty\sqrt{\pi c}\,(\sin^2\beta + \lambda\cos^2\beta)\sin^2\alpha$ $K_{II} = \sigma_y^\infty\sqrt{\pi c}\,(1 - \lambda)\sin\beta\cos\beta\sin\alpha$ (14) $K_{III} = \sigma_y^\infty\sqrt{\pi c}\,(\sin^2\beta + \lambda\cos^2\beta)\sin\alpha\cos\alpha$
I + II + III	Fig.6	where $\lambda = \sigma_x^\infty / \sigma_y^\infty$ σ_x^∞ and σ_y^∞ : applied stress in the x- and y-direction, respectively α and β : inclined angle of notch to the plate surface and y-axis, respectively

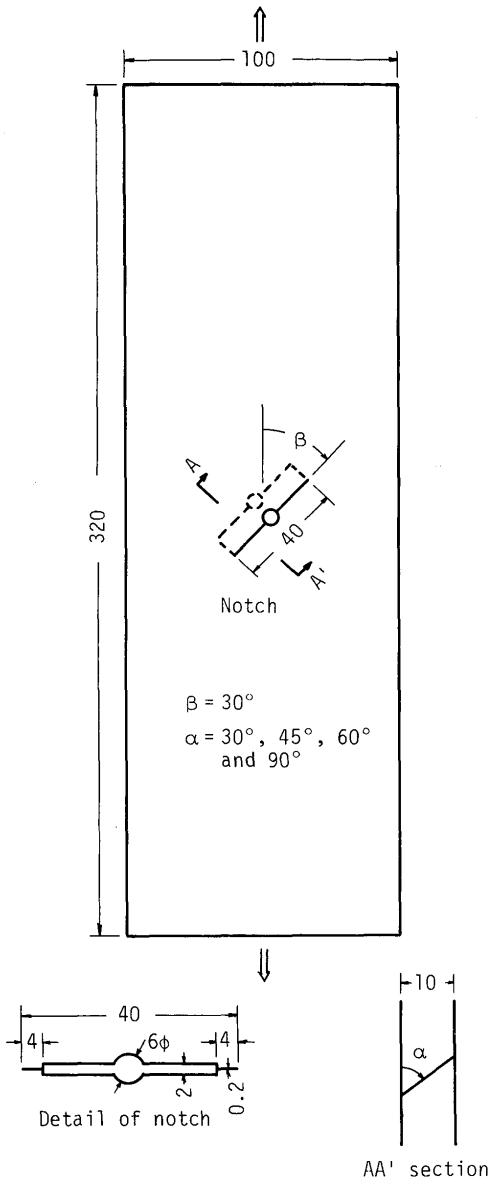

Fig. 6 Plate specimen for test under combined modes of I, II and III

3.3 Test procedure

Fracture tests under uni-axial tension and bending are carried out using the 10 tons testing machine of a displacement control type, and those under bi-axial tension are carried out using this testing machine with combination of a specially designed loading frame of a screw type[1)2)].

The mean stresses, σ_{xe} and σ_{ye}, surrounding the notch in the cruciform specimen are different from those along the loading edges, σ_x and σ_y. The relation between these stresses are obtained by the stress analysis using the finite element method in the previous reports,[1)2)] and is expressed in the following form.

$$\begin{Bmatrix} \sigma_{xe} \\ \sigma_{ye} \end{Bmatrix} = \begin{bmatrix} 0.80 & -0.09 \\ -0.09 & 0.80 \end{bmatrix} \begin{Bmatrix} \sigma_x \\ \sigma_y \end{Bmatrix} \quad (15)$$

The stress intensity factors of the notch in the cruciform specimen can be obtained by Eq. (14) substituting σ_{xe} and σ_{ye} into σ_x^∞ and σ_y^∞, respectively.

The fracture tests are carried out at room temperature, and the direction of the initial crack propagation and the fracture loads are measured. Bi-axial tensile loads are applied proportionally in both directions, of which load ratios are 1/2 and 1/1.

4. Test Results and Discussions

4.1 Pure Mode II

The fracture toughness value, K_c, of PMMA was 4.6 kg/mm$^2\sqrt{\text{mm}}$ from the test on the conventional specimen of $\alpha = 90°$ in Fig. 5 (a).

As for the direction of the initial crack propagation, $-\theta_0$, and the ratio of K_{II} to K_c at fracture, K_{IIf}/K_c, the comparison between the predicted and measured ones under pure Mode II is made on **Table 3**. The fracture angles, $-\theta_0$, predicted by the existing criteria are nearly equal to those measured. However, the fracture angle is not a sensitive parameter to indicate the validity of the fracture criteria.

Table 3 Predicted and measured results of pure Mode II test

	Criterion or test specimen		-θ(°)	K_{IIf}/K_c
Theory	Maximum tangential stress, $[\sigma_\theta]_{max}$		71	0.87
	Maximum energy release rate, $[G^k(\gamma)]_{max}$	Bilby *et al.*[7]	75	0.81
		Hussain *et al.*[10]	75	0.63
	Maximum energy release rate, $[G(\gamma)]_{max}$		72	0.75
Experiment	Plate specimen with curvilinear crack		82	0.91
	Beam specimen with edge cracks		68 73	0.74 0.78

-θ : direction of initial crack propagation
K_{IIf} : stress intensity factor of Mode II at fracture
K_c : fracture toughness

In contrast with this, the predicted fracture strengths by the various criteria vary to a great extent. For example, the predicted value of K_{IIf}/K_c based on $[\sigma_\theta]_{max}$ criterion is 1.38 times that based on $[G^k(\gamma)]_{max}$ by Hussain et al[11)] According to the test results of the beam specimen, the fracture angle as well as the strength ratio agree well with the estimates on the basis of $[G(\gamma)]_{max}$ criterion developed in this study. On the other hand, those of the plate specimen with a curvilinear notch are not precicted well by any criteria.

According to the experimental study by Shah[16] on the fracture of pure Mode II of the cylinderical pipes with a through-thickness circumferential crack which were fabricated from AISI 4340 and subjected to torsion, the test results showed that $-\theta_0 = 70 \sim 75°$ and $K_{IIf}/K_c = 0.92$ at fracture.

4.2 Pure Mode III

The ratio of K_{III} to K at fracture, K_{IIIf}/K_c, predicted by $[\sigma_\theta]_{max}$, $[G^k(\gamma)]_{max}$ and $[G(\gamma)]_{max}$ criteria are 1.0, 0.81 and 0.84, respectively. Meanwhile, the test results for two specimens indicate that the values of K_{IIIf}/K_c are 0.93 and 1.04. Then, it is seen that $[\sigma_\theta]_{max}$ criterion predicts best the results. However, it is a future problem to take account of the real distribution of shear stresses since the shear stress is regarded constant as in Eq. (13). The fracture initiated from some part of the notch front which cover about 5 mm from the top and bottom surface of the test specimen in Fig. 4 (b), and propagated through the width of the beam, After that, the fracture of Mode II prevailed at the newly created crack front and the test specimen fractured completely.

According to the experimental study after Shah[16] on the fracture of pure Mode III using the circumferentially notched round bar of AISI 4340 steel which was subjected to torsion, the test results presented that $K_{IIIf}/K_c = 0.96$.

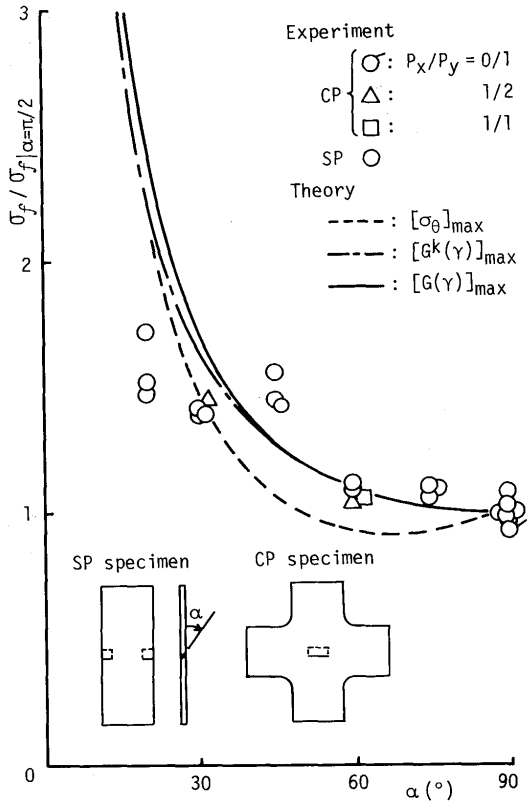

Fig. 7 Fracture stress under combined modes of I and III

4.3 Combination of Modes I and III

As for the fracture strength under the combination of Modes I and III, the test results were compared with the estimated in **Fig. 7**. The load ratio has little effects on the fracture strength. That is, the effect of uniform stress parallel to the notch on the fracture strength under the combination of Modes I and III ($\beta = 90°$) can be hardly observed from the test results as well as Eq. (14), in the same manner as the case of the combination of Modes I and II[1)2)].

In the range of small α, there is a difference in fracture strength between the measured one and the estimated one calculated by any criteria. The main reason for this difference may be attributed to the assumption which was used in the derivation of Eq. (14), that is, the stress and deformation through the plate thickness is uniform. However, the assumption is no longer valid in such a range of α on account of the finite thickness, and consequently K-formulae can not be expressed accurately by Eq. (14). Meanwhile, in the range or large α, the estimated results by $[G^k(\gamma)]_{max}$ and $[G(\gamma)]_{max}$ criteria excluding $[\sigma_\theta]_{max}$ one agree well with the experimental results.

The examination of the fractured specimens revealed that in the range of $\alpha > 60°$, the fracture initiated from all part of the notch front and propagated perpendicularly to the plate surface with the crack surface being twisted. Meanwhile, in the range of $\alpha < 60°$, the fracture initiates only from one point of the notch front and within a small distance the crack plane is twisted perpendicularly to the plate surface. Therefore, the fracture surface and the notched one intersect at a point of the notch tip. As α decreases, this tendency becomes more evident and the point of the fracture initiation on the notch front approaches to the plate surface. The fracture behaviors under the combination of Modes I and III were studied on a bar of AISI 4340 steel by Shah[16]. In his experiment, the circumferentially notched round bar was subjected to tension and torsion under proportional loading. The test results were plotted as the interaction curve between K_{If} and K_{IIIf}. It was found from the curve that K_{III} has little effect on the fracture strength in the range of $K_{IIIf}/K_c < 0.7$. The trends of this curve are much defferent from those shown later in **Fig. 10**. Also, the effect of K_{III} on fracture strength was studied on similar specimens to that of Fig. 5 (a) for aluminum alloy and tool steel by Pook[17],

and for mild steel and 80kg/mm^2 high strength steel by Sakai and Sakano[18]. Both test results showed that K_{III} had little effect on the fracture strength in the range of 45°< <90°. These trends are different from those in Fig. 10. This disagreement may be attributed to the fact that the material tested is perfectly brittle one such as PMMA or semi-brittle one such as alloy and steel.

4.4 Combination of Modes I, II and III

The fracture stresses obtained by the test are shown in Fig. 8 in comparison with the estimates by $[G^k(\gamma)]_{max}$

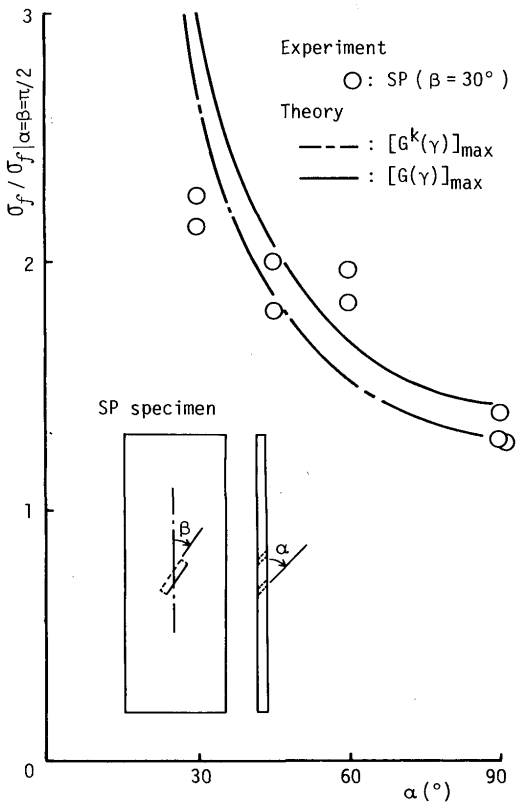

Fig. 8 Fracture stress under combined modes of I, II and III

and $[G(\gamma)]_{max}$ criteria. The fracture stress increases with a decrease of α, and the estimates agree with the test results except in the range of small α. The cause for this difference in small α is the same as that stated previously in 4.3. The behaviors of the fracture initiation and propagation are nearly similar to that under the combination of Modes I and II.

4.5 Interaction curves on fracture strength under combined modes

The interaction curves of K_{If}/K_c, K_{IIf}/K_c and K_{IIIf}/K_c at fracture under the combination of Modes I, II and III can be obtained by applying individual fracture criteria. The interaction curves under the combinations of Modes I and II, and I and III are shown in Figs. 9 and 10, respec-

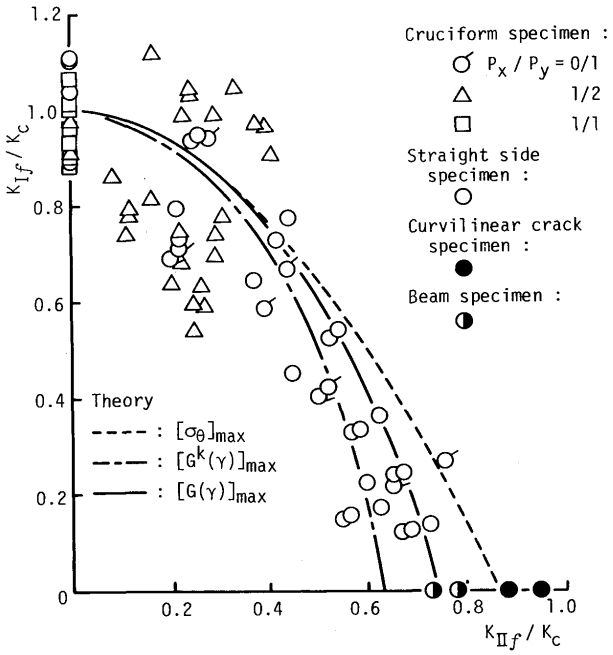

Fig. 9 Interaction curves of K_{If} and K_{IIf}

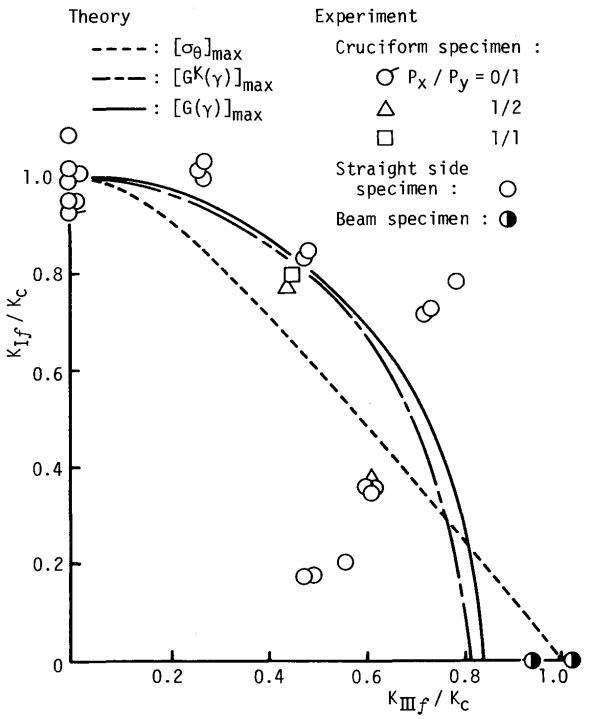

Fig. 10 Interaction curves of K_{If} and K_{IIIf}

tively. In these figures, the results of the previous tests[1)2)] as well as the present ones are plotted. Although the test results scatter considerably as observed in Fig. 9, most test points are plotted in a small width of the estimated lines calculated by $[G^k(\gamma)]_{max}$ and $[G(\gamma)]_{max}$ criteria. It is also found from Fig. 10 that those estimated by $[G^k(\gamma)]_{max}$ and $[G(\gamma)]_{max}$ criteria agree with the measured ones except in the range of the small value of K_{III}/K_I which corresponds to that of small α.

Then, the interaction curves under the general combined modes are obtained only based on $[G^k(\gamma)]_{max}$ and $[G(\gamma)]_{max}$ criteria and they are shown in **Figs. 11** and **12**, respectively. In fact, the group of those curves forms the curved surface in the coordinates of K_{If}/K_C, K_{IIf}/K_C and K_{IIIf}/K_C. The fracture strength can be estimated from the interaction surface as the coordinate of the intersecting point of the curved surface by the line drawn from the origin, of which the direction consines are proportional to the specified values of K_I, K_{II} and K_{III}, respectively. Moreover, the estimated fracture strength by $[G^k(\gamma)]_{max}$ criterion is more conservative than that by $[G(\gamma)]_{max}$ one.

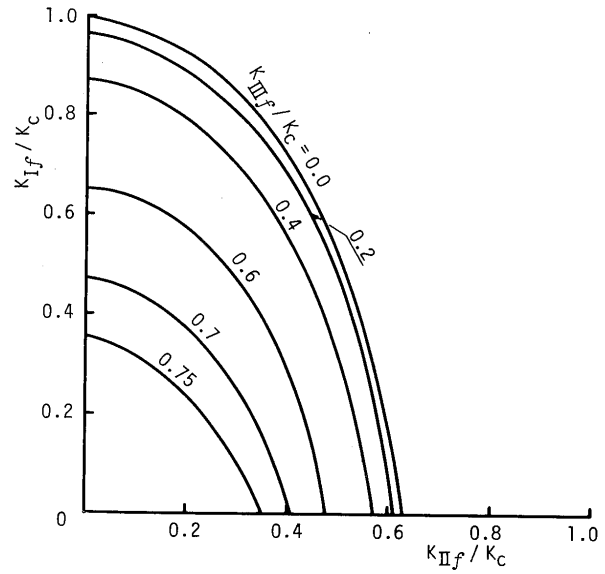

Fig. 11 Interaction curves of K_{If}, K_{IIf} and K_{IIIf} predicted by $[G^k(\gamma)]_{max}$ criterion

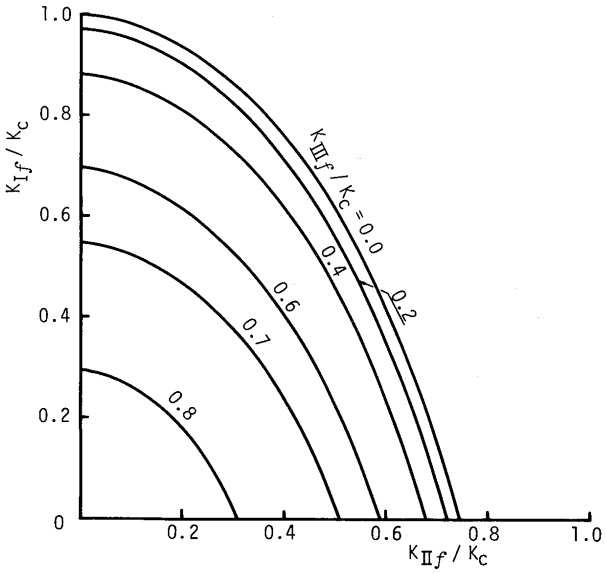

Fig. 12 Interaction curves of K_{If}, K_{IIf} and K_{IIIf} predicted by $[G(\gamma)]_{max}$ criterion

5. Conclusions

The brittle fracture initiation characteriatics under arbitrary combination of Modes I, II and III were investigated. Firstly, the newly developed fracture criterion, which is based on the approximate energy ralease rate at the instant when the kinked crack initiated from the tip of the main crack, $[G^k(\gamma)]_{max}$, was proposed. Secondary, the fracture criterion based on the tangential stress at the crack tip, $[G(\gamma)]_{max}$, was extended for the general combined modes including Mode III.

The following conclusions are drawn from the comparison between the theory and the test results:

(1) The measured fracture stresses under an arbitrary combination of the crack surface displacement modes are in good agreement with those predicted by $[G^k(\gamma)]_{max}$ or $[G(\gamma)]_{max}$ criterion. $[G^k(\gamma)]$ is the energy release rate at the propagation from a small kinked crack. These energy release rates are expressed in the closed forms, and can be applied to any crack under arbitrary combination of modes.

(2) Although $[\sigma_\theta]_{max}$ criterion may be used for fracture of any combined modes including Mode III, this may not be an effective criterion except for the combination of Modes I and II.

(3) The interaction curves of fracture strength under any arbitrary combination of Modes I, II and III are obtained based on $[Gk(\gamma)]_{max}$ and $[G(\gamma)]_{max}$ criteria.

References

1) Y. Ueda, K. Ikeda, T. Yao, M. Aoki, T. Yoshie and T. Shirakura : Brittle Fracture Initiaion Characteristics under Bi-axial Loading, J. Soc. Naval Arch. of Japan, Vol. 139 (1976), pp. 240 - 247, (in Japanese).

2) Y. Ueda, K. Ikeda, T. Yao, M. Aoki, T. Yoshie and T. Shirakura : Brittle Fracture Initiation Characteristics under Bi-axial Loading, Fracture, Vol. 2, ICF4, Waterloo, Canada (1977), pp. 173 - 182.

3) Y. Ueda, K. Ikeda, T. Yao, M. Aoki, T. Yoshie, T. Shirakura and S. Shibasaki : Brittle Fracture Initiation Characteristics under Bi-axial Loading (2nd Report) – in case of large scale

and general yeilding state – , J. Soc. Naval Arch. of Japan, 142 (1977), pp. 127 - 134, (in Japanese).

4) Y. Ueda, K. Ikeda, T. Yao, M. Aoki, T. Yoshie, T. Shirakura and S. Shibasaki : Brittle Fracture Initiation Characteristics under Bi-axial Loading (2nd Report) – in case of large scale and general yielding state – , Trans. JWRI, Vol. 8, No. 1(1979), pp. 121 - 130.

5) F. Erdogan and G. C. Sih : On the Crack Extension in Plates under Plane Loading and Transverse Shear, Trans. ASME, J. Basic Eng., 85D (1963), pp. 519 - 527

6) J. G. Williams and P. D. Ewing : Fracture under Complex Stress – The Angled Crack Problem, Int. J. Frac. Mech., Vol. 8, No. 4(1972), pp. 441 - 446.

7) G. C. Sih and B. C. K. Cha : A Fracture Criterion for Three-Dimensional Crack Problems, Eng. Frac. Mech., 6(1974), pp. 699 - 723.

8) B. A. Bilby and G. E. Cardew : The Crack with Kinked Tip, Int. J. Frac. Mech., Vol. 11, No. 4 (1975), pp. 708 - 712.

9) A. A. Khrapkov : The First Basic Problem for a Notch at the Apex of an Infinite Wedge, Int. J. Frac. Mech., Vol. 7, No.4 (1971), pp. 373 - 382.

10) S. N. Chatterjee : The Stress Field in the Neighborhood of a Branched Crack in an Infinite Elastic Sheet, Int. J. Solid and Structures, Vol. 11 (1975), pp. 521 - 538.

11) M. A. Hussain, S. L. Pu and J. Underwood : Strain Energy Release Rate for a Crack under Combined Mode I and II, ASTM STP 560 (1974), pp. 2 - 28.

12) G. C. Sih : Stress Distribution near Internal Crack Tips for Longitudinal Shear Problems, Trans. ASME, J. Appl. Mech., March (1965), pp. 51 - 58

13) E. Smith : A Note on Crack-forming in Anti-Plane Strain Deformation, Int. J. Frac., Vol. 9, No.2 (1973), pp. 181 - 183.

14) G. C. Sih, P. C. Paris and F. Erdogan : Crack Tip Stress Intensity Factors for Plane Extension and Plate Bending Problems, Trans. ASME, J. Appl. Mech., Vol. 29 (1962), pp. 306 - 312.

15) M. A. Hussain and S. L. Pu : Slip Phenomenon for a Circular Inclusion, Trans. ASME, J. Appl. Mech., Vol. 38, No. 3 (1971), pp. 627 - 633.

16) R. C. Shah : Fracture under Combined Modes in 4340 Steel, ASTM STP 560 (1974), pp. 29 - 52.

17) L. P. Pook : The Effect of Crack Angle on Fracture Toughness, Eng. Frac. Mech., Vol. 3 (1971), pp. 205 - 218.

18) K. Sakai and K. Sakano : A Study on Brittle Fracture Initiation under Combined Modes, J. Soc. Naval Arch. of Japan, Vol. 139 (1976), pp. 257 - 264, (in Japanese).